nature communications

Article

https://doi.org/10.1038/s41467-024-51108-z

A broadly protective antibody targeting glycoprotein Gn inhibits severe fever with thrombocytopenia syndrome virus infection

Received: 15 February 2024

Accepted: 29 July 2024

Published online: 15 August 2024

Check for updates

Xuanxiu Ren[1,5], Jiawen Sun[2,3,5], Wenhua Kuang[2,5], Feiyang Yu[1], Bingjie Wang[1], Yong Wang[2,3], Wei Deng[2,3], Zhao Xu[2,3], Shangyu Yang[1], Hualin Wang[2,4], Yangbo Hu[2,4], Zengqin Deng[2,4] ✉, Yun-Jia Ning[2,4] ✉ & Haiyan Zhao[1] ✉

Severe fever with thrombocytopenia syndrome virus (SFTSV) is an emerging bunyavirus that causes severe viral hemorrhagic fever and thrombocytopenia syndrome with a fatality rate of up to 30%. No licensed vaccines or therapeutics are currently available for humans. Here, we develop seven monoclonal antibodies (mAbs) against SFTSV surface glycoprotein Gn. Mechanistic studies show that three neutralizing mAbs (S2A5, S1G3, and S1H7) block multiple steps during SFTSV infection, including viral attachment and membrane fusion, whereas another neutralizing mAb (B1G11) primarily inhibits the viral attachment step. Epitope binning and X-ray crystallographic analyses reveal four distinct antigenic sites on Gn, three of which have not previously been reported, corresponding to domain I, domain II, and spanning domain I and domain II. One of the most potent neutralizing mAbs, S2A5, binds to a conserved epitope on Gn domain I and broadly neutralizes infection of six SFTSV strains corresponding to genotypes A to F. A single dose treatment of S2A5 affords both pre- and post-exposure protection of mice against lethal SFTSV challenge without apparent weight loss. Our results support the importance of glycoprotein Gn for eliciting a robust humoral response and pave a path for developing prophylactic and therapeutic antibodies against SFTSV infection.

Severe fever with thrombocytopenia syndrome virus (SFTSV) is a tick-borne bunyavirus that causes severe hemorrhagic fever, leukopenia, thrombocytopenia, and multiple organ failure (SFTS) in humans, which belongs to the genus *Bandavirus* under the family of *Phenuiviridae*[1–3]. Since it was first discovered in China in 2009, the number of SFTSV infection cases has been increasing annually in East Asia, including South Korea, Japan, China, Vietnam, Pakistan, and Thailand, with a fatality rate of up to 30%[1,4]. Although SFTSV mainly emerges in the Asian continent so far, the Asian longhorned tick, which is believed to be the primary tick vector transmitting SFTSV[5], has been detected in the United States, Russia, Australia, and the Western Pacific regions[6–8], raising the concern about the future emergence of SFTSV outside of the Asian countries. Despite the severity of SFTS disease, approved vaccines and specific therapeutics against SFTSV are currently unavailable[9]. SFTSV has also been listed as one of the prioritized pathogens by the World Health Organization (WHO) in 2018, underscoring the need for more research and efforts to develop antivirals and vaccines against this pathogen.

SFTSV is closely related to two novel tick-borne bunyaviruses: one is the heartland virus (HRTV), which primarily emerges in the United

[1]State Key Laboratory of Virology, College of Life Sciences, Wuhan University, Wuhan, Hubei, China. [2]Key Laboratory of Virology and Biosafety, Wuhan Institute of Virology, Chinese Academy of Sciences, Wuhan, Hubei, China. [3]University of Chinese Academy of Sciences, Beijing, China. [4]Hubei Jiangxia Laboratory, Wuhan, Hubei, China. [5]These authors contributed equally: Xuanxiu Ren, Jiawen Sun, Wenhua Kuang ✉e-mail: dengzengqin@wh.iov.cn; nyj@wh.iov.cn; hy.zhao@whu.edu.cn

States[10,11], and the other is the Guertu virus (GTV)[2,12]. HRTV infects humans with severe clinical symptoms, and viral-related deaths have occurred. Although no GTV-infected human cases have been reported, the cell-based assays showed that GTV could infect both animal and human cells, and a serological survey identified antibodies against GTV in human serum samples[12], suggesting the potential risk of GTV to infect humans.

SFTSV can be classified into six genotypes (A-F) based on their amino acid sequence[13,14]. Like most Bunyaviruses, SFTSV is an enveloped, negative-sense single-stranded RNA virus that carries three gene segments, designated the large (L), medium (M), and small (S). The M segment encodes a precursor glycoprotein post-translationally cleaved by host protease into two envelope proteins, Gn (the N-terminal half) and Gc (the C-terminal half). Recently, two modest-resolution cryo-EM structures of SFTSV virion revealed that Gn and Gc form heterodimers covering the viral surface[15,16], which mediate viral attachment, entry, and fusion[17,18]. SFTSV Gn is a type I transmembrane protein and reported to interact with host receptors/factors for viral binding and entry[17,19]. The N-terminal region of Gn ectodomain (residues 20-340), designated Gn head, exists as a triangular shape and can be further divided into three major segments: domain I (DI), domain II (DII), and domain III (DIII)[20]. Vaccine developments based on SFTSV Gn alone or in combination with Gc displayed protection efficiency against SFTSV infection in distinct animal models[21–25], which induce strong humoral and cellular immune responses. Furthermore, anti-SFTSV neutralizing antibodies that recognize Gn have been described, suggesting that Gn is a potential target for neutralizing antibodies[20,26–28].

So far, only three SFTSV Gn-specific mAbs have been reported. The binding epitope of MAb4-5 has been revealed by crystal structure[20]; however, MAb4-5 provided poorly protective activity in vivo[26]. Although antibodies Ab10 and SNB02 showed promising in vivo protective effects against SFTSV challenge, the precise binding footprints of these two mAbs are unknown[26,28]. Therefore, comprehensively characterizing the antigenic features of the glycoprotein Gn and developing novel protective antibodies are important for vaccine design and therapeutic development to combat SFTSV infection.

In this study, we developed seven Gn-specific mouse mAbs against SFTSV after immunizing with recombinant Gn head protein or chimeric SFTSV pseudovirus (rVSV-eGFP-SFTSV) and boosting with recombinant Gn protein. These mAbs fall into four competition-binding groups with neutralizing infection of SFTSV to varying degrees. Of these, three groups, including a total of six mAbs, recognize previously unreported epitopes on Gn. Crystal structures of SFTSV Gn head in complexed with representative Fabs from these three novel groups reveal the antigenic sites and correlation between mAbs epitopes and neutralizing activities. Importantly, our structural data, combined with mechanism of action and in vivo protection studies, demonstrate that the most potently neutralizing mAb (S2A5) recognizes Gn domain I, prevents viral attachment and membrane fusion, and displays prophylactic and therapeutic protection against lethal SFTSV infection in mice. These results define a critical neutralization epitope on the surface of SFTSV Gn glycoprotein and provide the molecular basis for neutralizing SFTSV infection by mAbs.

Results

Generation and characterization of mAbs against SFTSV glycoprotein Gn

BALB/c mice were immunized with purified Gn head protein mixed with AddaVax or infectious rVSV-eGFP-SFTSV four or three times, and these mice were then boosted with 25 μg purified Gn head protein before the B cell isolation (Supplementary Fig. 1a, d). The serum neutralizing capacity of the immunized mice was evaluated against SFTSV genotypes A (strain WCH97) and D (strain QD02) pseudoviruses. An NT_{50} (half-maximal neutralizing dilutions) of >1/10,000 was observed for the serum of mice immunized with infectious rVSV-eGFP-SFTSV (Supplementary Fig. 1e). For recombinant Gn-immunized mice, the sera displayed varying inhibitory activities as only one mouse serum showed strong neutralizing potency with an NT_{50} value of ~1/10,000, and other three mice displayed weak neutralizing activity against both SFTSV genotypes A and D pseudotyped viruses (Supplementary Fig. 1f).

We then sorted single Gn-binding B cells by flow cytometry and conducted antibody cloning and sequencing (Supplementary Fig. 1g). The paired variable genes of heavy chain and light chain were cloned into human IgG1 expression vectors and expressed in Expi293 cells. The reactivity of purified mAbs to SFTSV, HRTV, and GTV Gn head proteins (Supplementary Fig. 1a–c) was tested by enzyme-linked immunosorbent assay (ELISA) (Fig. 1a). Seven SFTSV Gn-binding mAbs (S1G3, S2A5, S1E9, N1D10, S1H7, N1C3, and B1G11) were identified, of which, five mAbs (S2A5, S1E9, N1D10, S1H7, and B1G11) showed diverse reactivity with Gn of GTV, and two mAbs (S1E9 and N1D10) could also cross-recognize HRTV Gn. The half maximal effective binding concentrations against SFTSV Gn are hard to obtain for mAbs S2A5 and S1G3, indicating that these two mAbs weakly bind to solid phase recombinant SFTSV Gn protein. To evaluate the binding features of these mAbs further, we tested the reactivity of these mAbs to authentic SFTSV virions and found that all seven mAbs can bind intact, authentic virions (Fig. 1b). In this setting, the maximal binding activity of S2A5 is slightly higher than other mAbs, indicating that S2A5 prefers to bind virus particles. The disparities in the binding to recombinant protein versus intact virion have also been reported for mAbs against distinct viruses, including flaviviruses[29] and alphaviruses[30,31]. This might reflect epitope environment differences between recombinant protein and authentic viral particle. For instance, some complex quaternary epitopes exist exclusively on the whole virion, while some fully accessible epitopes on the recombinant antigen are hidden or partially hidden on the virion.

Neutralizing activity and breadth of the mAbs

To evaluate the inhibitory activity of these mAbs, we first performed a SFTSV pseudovirus neutralization assay. Three (S1G3, S2A5, and S1H7) of the seven mAbs displayed efficient neutralizing activity with half-maximal inhibitory concentrations (IC_{50}) smaller than 6.0 ng/mL against the infection of SFTSV QD02 pseudotyped virus, and B1G11 exhibited moderate neutralization activity (IC_{50} = 53.1 ng/mL), whereas the other three mAbs (S1E9, N1D10 and N1C3) showed weak or no neutralizing ability (Fig. 1c). We further assessed the neutralizing breadth of these mAbs using SFTSV pseudoviruses encompassing the other five SFTSV genotypes. The most potent mAbs (S2A5, S1G3, and S1H7) can efficiently inhibit pseudotyped SFTSV infection across all six genotypes (Fig. 1c–h and Table 1). Consistent with the SFTSV pseudovirus neutralizing results, the three potent mAbs exhibited highest inhibitory potency against authentic SFTSV strains QD02 ($IC_{50} \le 0.35$ μg/mL) and WCH97 ($IC_{50} \le 0.05$ μg/mL). While B1G11 inhibited authentic SFTSV QD02 and WCH97 strains infection with IC_{50} values of 8.77 and 0.47 μg/mL, respectively (Fig. 1i, j and Table 1). N1C3, S1E9, and N1D10 could not appreciably neutralize authentic SFTSV QD02 or WCH97. In addition, the inconsistent neutralization sensitive between the pseudotyped and authentic SFTSV were observed, indicating that VSV-based SFTSV pseudovirus cannot completely mimic the surface glycoprotein arrangement of authentic SFTSV, as seen for hantavirus[32].

MAbs recognize four distinct antigenic sites on Gn

To investigate the antigenic regions recognized by the mAbs, we performed a competition-binding assay by biolayer interferometry (BLI). One previously reported anti-SFTSV MAb4-5 targeting the DIII of Gn was included for comparison[20]. The first mAb immobilized sensor was used to capture the recombinant SFTSV Gn head protein, and the binding capacity of the tested mAbs to the captured Gn was determined (Supplementary Fig. 2). This analysis showed that the seven

https://doi.org/10.1038/s41467-024-51108-z

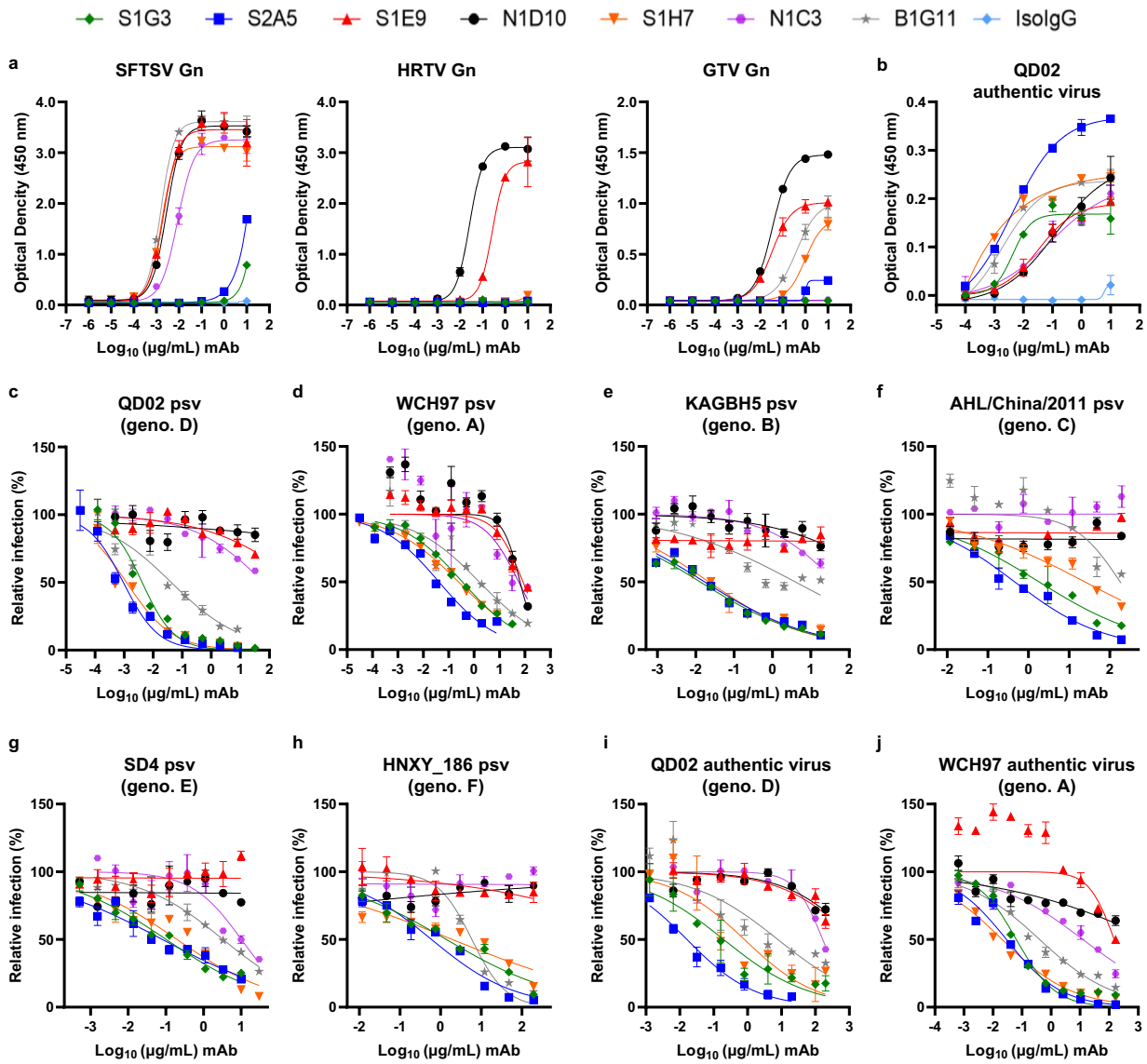

Fig. 1 | Binding and neutralizing capabilities of Gn mAbs. a, **b** The binding of mAbs to Gn head domain proteins (**a**) and authentic SFTSV QD02 (**b**) was assessed using ELISA. **c**-**h** The neutralization activity of Gn mAbs against SFTSV (genotypes A-F) pseudoviruses (psv). **i**, **j** Focus reduction neutralization tests (FRNT) against authentic SFTSV. Data represent mean ± SEM (standard error of the mean) of technical duplicates and are representative of two (**d**–**h**, **j**), three (**a**–**c**) or four (**i**) independent experiments. Source data are provided as a Source data file.

Table 1 | Neutralization potency of Gn mAbs

IC_{50} μg/mL[a]	Virus	SFTSV pseudovirus						Authentic SFTSV	
		WCH97 (geno.A)	KAGBH5 (geno.B)	AHL/China /2011 (geno.C)	QD02 (geno.D)	SD4 (geno.E)	HNXY_186 (geno.F)	WCH97 (geno.A)	QD02 (geno.D)
Gn mAb	S1G3	0.5153	0.0184	2.5680	0.0060	0.0787	2.3770	0.0510	0.2523
	S2A5	0.0423	0.0125	0.5345	0.0006	0.1132	0.6239	0.0228	0.0402
	S1E9	83.9700	>100	>100	>100	>100	>100	76.5830	>100
	N1D10	>100	>100	>100	>100	>100	>100	>100	>100
	S1H7	0.2509	0.0136	21.3250	0.0031	0.3208	3.3370	0.0334	0.3528
	MAb4-5[b]	0.5917	0.0529	>100	0.0426	0.4667	2.5665	NT	6.3310
	N1C3	56.6500	36.0700	>100	92.8700	20.4150	>100	14.7050	>100
	B1G11	3.7275	4.7775	>100	0.0531	4.8975	6.6510	0.4703	8.7737

[a]The neutralization potency of mAb against pseudotyped or authentic SFTSV is summarized. NT, not detected. The IC_{50} values are the average of two to four independent experiments and are determined by non-linear regression. [b]MAb4-5 is a previously reported antibody that recognizes the SFTSV Gn protein.

mAbs can be classified into four competition groups (groups A-D). Among them, mAb S1H7 competed with MAb4-5 for the Gn binding (group C), and the binding of S2A5 to Gn excluded the interaction of Gn with S1G3. This suggests that S2A5 and S1G3, both potently neutralizing mAbs, are in the same group and recognize overlapping regions on Gn (group A), while S1H7 and MAb4-5 belong to another group. The broadly cross-reactive mAbs (N1D10 and S1E9) are grouped together (group B), whereas B1G11 (intermediate neutralizing capacity) and weak-neutralizing mAb N1C3 are categorized into group D (Fig. 2a).

The binding affinity between the mAbs and recombinant Gn head protein was also assessed by BLI (Fig. 2b). The data showed that moderately neutralizing mAb B1G11 had the highest binding affinity with a kinetic binding affinity (K_D) around 0.19 nM and half-live (t1/2) over 220 min. Compared to B1G11, the other three potently inhibitory mAbs in our panel gave relatively lower binding affinities, S2A5 had a K_D of 3.25 nM and t1/2 of 11.59 min, S1G3 had a K_D of 13.3 nM and t1/2 of 1.46 min, and S1H7 had a K_D of 2.03 nM and t1/2 of 20.20 min. The other three weak/no neutralizing mAbs gave affinities of ~15 nM. Thus, it appears that the binding affinity of the mAbs to the purified protein alone cannot precisely predict the antibodies' neutralizing potency, as seen with mAbs against distinct viruses[33,34].

Neutralizing mechanisms of Gn mAbs

To elucidate the inhibition mechanisms of these mAbs, we focused on four potent mAbs, including S2A5, S1G3, S1H7, and B1G11. Viral attachment blocking assay was performed by pre-incubating tested mAbs or an isotype control mAb with authentic SFTSV QD02 virus (genotype D), and then the mixtures were added to Vero E6 cells for the binding step at 4 °C. After extensive washing, cell-bound viral RNA was detected by quantitative real-time PCR (qRT-PCR). Compared to the isotype control, B1G11 reduced ~50% virus attachment at a concentration of 10 μg/mL, which is close to the IC_{50} of B1G11 (8.77 μg/mL). The attachment was blocked ~76% by S1G3, ~81% by S2A5, and ~76% by S1H7 at a concentration of 10 μg/mL, which is ~30- to 250-fold higher than the IC_{50} values of these mAbs. Expectedly, the attachment inhibition effect increased when 100 μg/mL of mAbs were used for all four mAbs (Fig. 3a).

To corroborate the results, pre- and post-attachment neutralization capacities were investigated (Fig. 3b). The results showed that all the four neutralizing mAbs could inhibit authentic SFTSV QD02 infection when pre-mixed the mAbs with the virus, and the IC_{50} (pre) values were close to the IC_{50} determined by a standard neutralizing assay in which mAbs existed throughout the infection. After virus adsorption to the cell surface, the addition of S2A5, S1G3, or S1H7 still greatly limited SFTSV infection, although a slight reduction in neutralization potency was observed compared to the pre-attachment neutralization setting, suggesting that the three mAbs could also work at a post-attachment step.

We next tested whether the four neutralizing mAbs could inhibit viral fusion, which is a crucial post-attachment step in the virus lifecycle (Fig. 3c). To measure the fusion inhibitory effects, we performed an SFTSV M-mediated cell-cell fusion assay, and acid-induced membrane fusion was monitored by a dual functional split reporter protein (DSP, renilla luciferase [Luc] and green fluorescent protein [GFP]). 293T cells expressing SFTSV M and reporter plasmid A (DSP1-7) were mixed with 293T cells expressing SFTSV M and reporter plasmid B (DSP8-11) for 24 h to allow the binding of M-encoding glycoproteins with cellular receptors, then the cells were incubated with tested mAbs or an isotype control mAb for 2 h. After washing to remove unbound mAbs, SFTSV M-mediated cell-cell fusion was triggered by brief exposure of the cells to an acidic medium (pH 5.0), and the fusion activity was measured at ~24 h after acid treatment. We found that S2A5, S1G3, and S1H7 significantly reduced the pH-triggered M-mediated membrane fusion, whereas mAb B1G11 and isotype control mAb did not show any fusion blockade activity at all tested concentrations. Consistently, at acidified condition (pH 5.0), all four mAbs (S2A5, S1G3, S1H7, and B1G11) retained strong binding to the recombinant Gn head protein with affinities varying from 1.67 pM to 43.5 nM (Supplementary Fig. 3 and Supplementary Table 6). Taken together, these results suggest that three potently neutralizing mAbs can inhibit both SFTSV attachment and fusion steps, while modest inhibitory mAb B1G11 primarily functions at a viral attachment step.

Structures of SFTSV antibodies in complex with Gn

To delineate the molecular basis of mAbs function, we determined crystal structures of Gn head complexed with the representative Fab from three distinct groups: S2A5 Fab-Gn complex to 2.45 Å resolution, B1G11 Fab-Gn complex to 3.05 Å resolution, and N1D10 Fab-Gn complex to 3.52 Å resolution (Supplementary Table 1 and Supplementary Fig. 7). Compared to the previously determined crystal structure, binding of mAbs to Gn did not lead to noticeable conformational change to Gn, with a root mean square deviation (r.m.s.d.) ranging from 0.5 to 0.7 Å. Structural analysis showed that S2A5 (group A) binds to the DI of Gn, while B1G11 (group D) binds to the DII of Gn (Fig. 4a, b). Despite N1D10 (group B) contacting both DI and DII (Fig. 4c), it approaches the DII from the opposite side compared to B1G11. Although three residues in DI are contacted by both S2A5 and N1D10 (Supplementary Fig. 4), binding of these two Fabs to Gn is compatible without clash observed when the S2A5 Fab-Gn and N1D10 Fab-Gn structures were superposed (Fig. 5a). Consistent with our competition-binding results, the three mAbs have distinct antigenic epitopes on Gn.

S2A5 interacts with 17 residues on the DI of Gn, including 9 residues (H64, Q66, K111-G114, D116, W141 and R149) contacted by heavy chain, 5 residues (K147, T150, S152, S157, and S158) contacted by light chains and 3 residues (E154-C156) interacted by both heavy and light chains (Supplementary Fig. 4 and Supplementary Table 2). The total buried surface areas of S2A5 and Gn in the complex are ~861 $Å^2$ and 860 $Å^2$, respectively (Fig. 4d). The heavy chain accounts for ~63% of the interface, with all three heavy chain complementarity-determining regions (CDR-H1, CDR-H2, and CDR-H3) involved in the interaction. Tight binding is facilitated by 18 hydrogen bonds, of which heavy chains (S30, D31, D32, D52, R94, Y98, G99, and R100A) contribute 13 hydrogen bonds. Two light chain CDRs (CDR-L1 and CDR-L2) also participate in the interaction by forming 5 hydrogen bonds with residues K147, T150, S152, C156, and S158 from Gn.

B1G11 contacts a DII region constituted by 10 residues on two discontinuous polypeptide elements: 7 residues (P185 to T190 and E193) in or adjacent to one large helix and 3 residues (M321 to V323) in one strand of Gn (Fig. 4e, Supplementary Fig. 4 and Supplementary Table 3). Five CDRs (CDR-H1, CDR-H2, CDR-H3, CDR-L1, and CDR-L3) contribute to the interaction, with heavy chain contributing ~61% buried surface area at the interface. For B1G11, 8 residues (Y33, R52, K53, R97, D99, D100, Y100B and Y100D) from the heavy chain and 7 residues (S30, Y32, Y91, S92, K93, F94 and R96) from the light chain contribute to the binding. CDR-H3 and CDR-L3 make extensive contacts with Gn by forming 6 hydrogen bonds with the residues (E188, E189, T190, and R322) from Gn; the other three hydrogen bonds are formed between residues from the CDR-L1 and CDR-H2 and the residues (P185 and E193) in Gn. The total buried surface areas of B1G11 and Gn in the interface are ~703 $Å^2$ and 706 $Å^2$, respectively.

N1D10 engages 8 residues (Y83, G114, D116, M117, I118, P120, G121 and E154) on DI and 16 residues (F202, D204, G218-D226, R241, R332, L337, V339 and S340) on DII of Gn (Fig. 4f, Supplementary Fig. 4 and Supplementary Table 4). The total buried surface area of S2A5 in the complex is ~1157 $Å^2$ with heavy chain contributing ~57% to the interaction, and Gn buried 1099 $Å^2$. Five CDRs (CDR-H1, CDR-H2, CDR-H3, CDR-L1, and CDR-L2) engaged in the interaction with the heavy chain predominantly binding DII, whereas the light chain contacts both DI and DII. Interestingly, the paratope is dominated by the CDR-H1, CDR-

https://doi.org/10.1038/s41467-024-51108-z

a

Antibody application			Second antibody							
	Competition group		A		B		C		D	
		mAb(Gn)	S1G3	S2A5	S1E9	N1D10	S1H7	MAb4-5	N1C3	B1G11
First antibody	A	S1G3	0.00	-0.50	33.69	65.23	78.09	86.96	85.37	100.00
		S2A5	4.35	0.00	41.10	67.21	75.40	82.41	86.49	100.00
	B	S1E9	37.90	27.28	0.00	11.46	69.78	71.93	84.78	100.00
		N1D10	76.74	80.21	2.12	0.00	66.34	77.60	83.29	100.00
	C	S1H7	88.35	76.21	64.38	72.17	0.00	2.63	84.72	97.16
		MAb4-5	86.89	92.22	69.71	84.85	-3.72	0.00	79.10	91.56
	D	N1C3	74.05	68.25	70.87	81.43	96.74	91.46	0.00	-6.58
		B1G11	77.63	86.05	64.34	92.22	82.65	88.16	-19.76	0.00

b

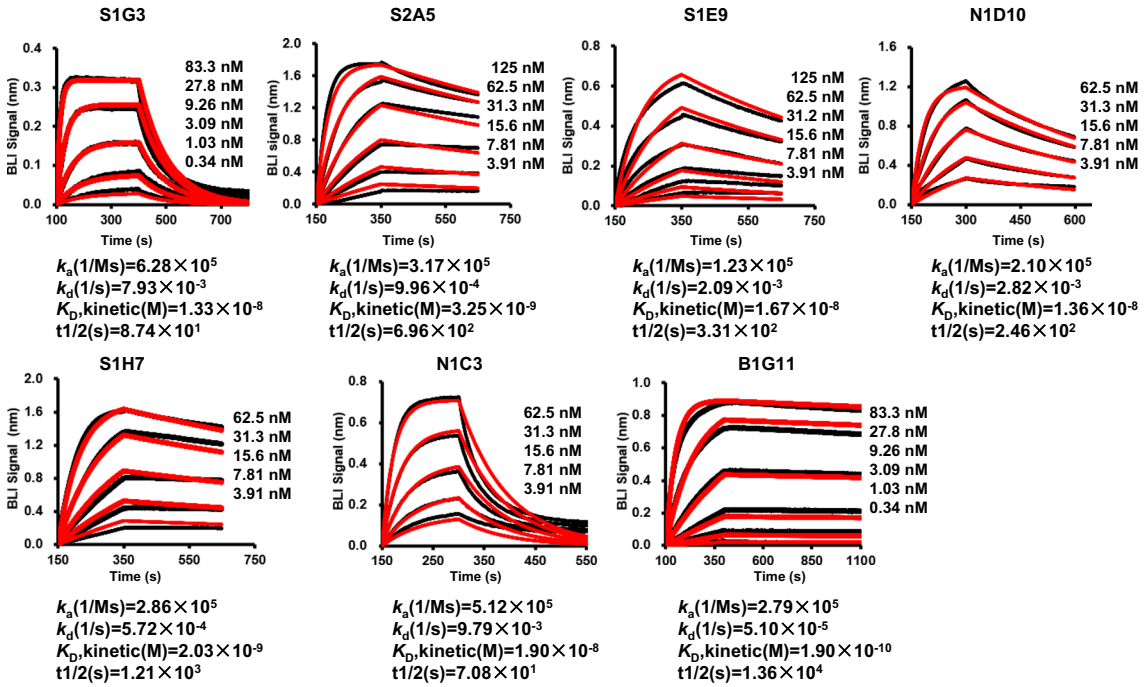

Fig. 2 | Binding affinity of Gn mAbs and competition-binding relationships. **a** Competition-binding assays were explored by BLI. The seven Gn mAbs were categorized into four groups (A, B, C, and D). The values in the table represent the percentage binding signal of tested antibodies in comparison to the binding signal of non-competitive antibodies. The antibodies were defined as strong competition if the percentage binding signal was less than 25%. MAb4-5 is a previously reported antibody that recognizes the SFTSV Gn protein. The results are averaged from two independent experiments. **b** The binding affinity of indicated mAbs to recombinant SFTSV Gn head protein was detected by BLI assay. Representative binding curves from two or three independent experiments. The values are the average of two to three independent experiments. The fitting curves are shown as red lines. Source data are provided as a Source data file.

H2, CDR-L1, and CDR-L2, accounting for 86% of contacts in contrast with the canonical CDR-H3/L3-dominated antibody/antigen interfaces. 12 hydrogen bonds form in the interface: CDR-H1 residues T28 and Y32, CDR-H2 residues N52A and S56 form 5 hydrogen bonds with Gn residues (D204, D226 and Y83); CDR-L1 residues (S30B, Y30C, and Y32), one CDR-L2 residue (S56) and Y49 form 6 hydrogen bonds with Gn residues (E154, D116, I118, P222, E119 and S340), and the other one is formed between S95 (CDR-H3) and Q223 of Gn.

The distinct SFTSV genotypes share >94% amino acid identity in the Gn proteins (Supplementary Fig. 1h). Sequence alignment analysis of representative SFTSV strains from six genotypes revealed that the epitope residues of S2A5 are strictly conserved across all six SFTSV genotypes (Supplementary Fig. 4). For the epitope of S2A5, SFTSV Gn has about 47% (8 out of 17) and 76% (13 out of 17) sequence identity to HRTV and GTV, respectively. For the B1G11 epitope, one different residue (V323I) in genotype C strain was observed among six SFTSV strains, and contacts on SFTSV Gn is 50% (5 out of 10) and 70% (7 out of 10) identity to HRTV and GTV, respectively. The binding footprints of N1D10 on Gn are 100% conserved among SFTSV genotypes C, D, E, and F, and variable positions in genotype B (Y83F and G218S) and genotype A (N340S) were observed. The epitope residues show 71% (17 out of 24) and 79% (19 out of 24) sequence identity with HRTV and GTV, respectively. These varying degrees of conservation of epitopes likely explain the differences in reactivity of the mAbs.

To test the critical interacting residues of the mAbs, we generated individual alanine substitution in SFTSV Gn expressing vector based on

https://doi.org/10.1038/s41467-024-51108-z

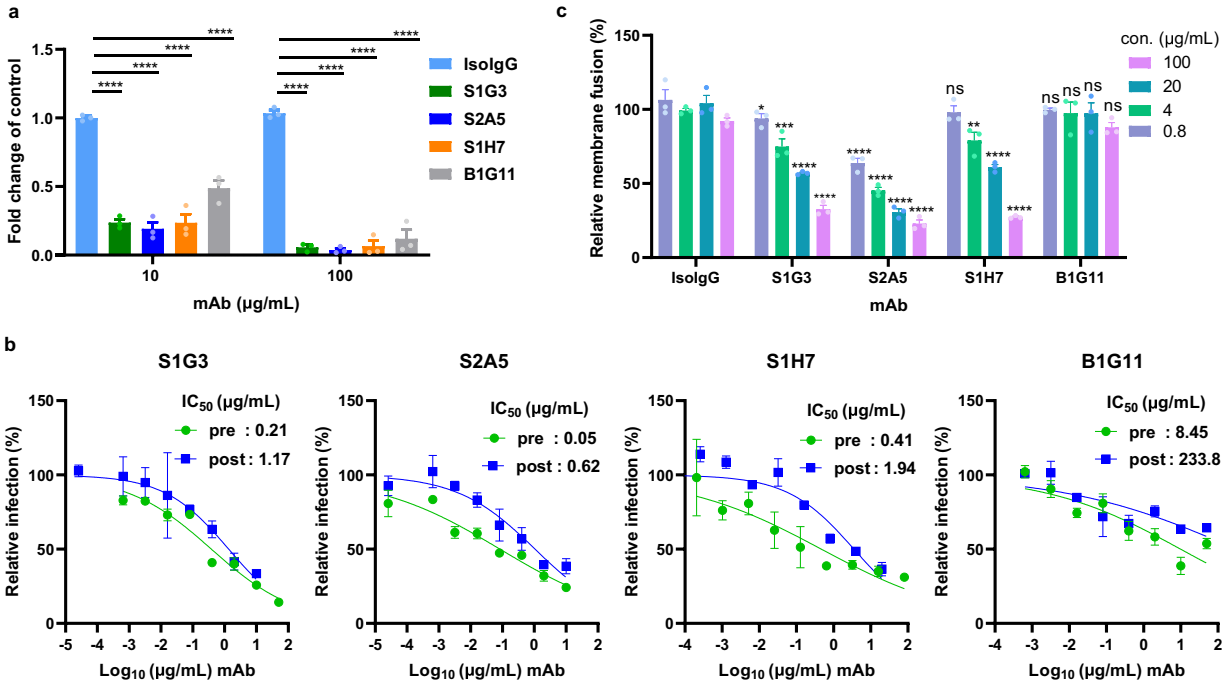

Fig. 3 | Neutralizing mechanism of Gn mAbs. a The inhibition of SFTSV attachment by mAbs at 10 or 100 μg/mL concentrations was assessed using qRT-PCR. GAPDH was used for internal control, and viral RNA fold change was compared with control cells incubated with Isotype IgG (NiV E2, anti-NiV mAb without binding to SFTSV, IsoIgG). Statistical significance was determined by a two-way ANOVA with Dunnett's multiple comparison tests in the comparison to IsoIgG group (****$p < 0.0001$). The data is mean ± SEM of three independent experiments performed in triplicate. **b** SFTSV pre-/post-attachment inhibition was assessed through FRNT assay. The IC_{50} values (indicated in the upper right corner) represent mean of three independent experiments performed in duplicate, with the green line representing pre-attachment inhibition curve and the blue line representing post-attachment inhibition curve. Data represent mean ± SEM of technical duplicates and are representative of three independent experiments. **c** The inhibition of membrane fusion induced by the SFTSV glycoprotein (encoded by segment M) was assessed using a split-GFP/Luc system, with live-cell luciferase activity being measured. Authentic SFTSV strain QD02 (genotype D virus) was used in a and b. The statistical significance was determined by comparing with the IsoIgG group at the same mAb concentration using Dunnett's multiple comparison tests in a two-way ANOVA analysis. The results for S1G3, S2A5, and S1H7 demonstrated a significant difference with $p < 0.0001$ (****), $p < 0.001$ (***), $p < 0.01$ (**), and $p < 0.05$ (*). Data represent mean ± SEM of three independent experiments performed in duplicate. Source data are provided as a Source data file.

the structurally defined epitopes of the three mAbs. The 293T cells were transfected with the wild-type (WT) or mutated plasmid, and the binding ability of the mAbs to Gn-expressing cells was determined by flow cytometry. The group A mAbs (S2A5 and S1G3) showed markedly decreased binding when alanine mutations were introduced at residues (H64, K111, R149, T150, and S152) within the S2A5 epitope. As expected, these mutations showed limited or no effect on the binding of Gn by the other six mAbs (Supplementary Fig. 5a). S1G3 also lost around 75% binding to cells expressing Gn-K113A, although this mutation had a minor effect on S2A5, indicating that the interaction modes of these two mAbs to Gn are not completely the same. Mutations of E188A, E189A, or E193A caused the loss of binding of group D mAbs (B1G11 and N1C3). Notably, the binding of N1C3 to Gn was also remarkably affected by the alanine substitution of T190, albeit this mutation did not show a significant effect on the interaction between Gn and B1G11 (Supplementary Fig. 5b). For group C mAbs, residues D204 and Q223 are critical for the binding of S1E9, but mutation of Q223A did not remarkably reduce the interaction of N1D10 with Gn, and N1D10 displayed reduced binding phenotypes to cells-expressing Gn-Y83A and Gn-D204A (Supplementary Fig. 5c). These findings are highly consistent with our competition-binding assay and structural analysis, further supporting that the isolated mAbs target four distinct antigenic determinants on Gn.

Exposed and cryptic SFTSV epitopes

Superimposition of B1G11, N1D10, MAb4-5, and S2A5-Gn complexes showed that four mAbs can simultaneously bind to Gn without steric clash (Fig. 5a). We next examined the accessibility of mAbs on the authentic SFTSV virions by superimposing the complex structures on an asymmetric unit (ASU) of the cryo-EM model of SFTSV virions (Fig. 5b–h). The SFTSV viral glycoprotein shell incorporates 720 Gn-Gc heterodimers, which are organized into ring-like penton and three types of hexon (peripentonal [hexon P], edge [hexon E], and central [hexon C])[15,16]. Each ASU constitutes 12 Gn-Gc heterodimers, including 1/5 of a penton, 1/3 of a hexon C, 1/2 of a hexon E, and a whole hexon P, which represents all possible assemblies of glycoproteins on the virion surface. Analysis of the docking results showed that the S2A5 epitope is exposed on the virion, while the B1G11 epitope is located on the side of the penton or hexon. In contrast, most of the N1D10 epitope is buried inside the pentameric and hexametric interface (Fig. 5c–e). The overall superimposition results from 12 Gn of one ASU are similar, and we here present the results of docking the complexes onto one Gn protomer of the hexon P. The analysis showed that B1G11 engages the DII with an approaching angle nearly parallel to the viral membrane, and the variable domain of B1G11 heavy chain appear to cause steric clashes with Gc from the adjacent Gn/Gc heterodimer within the same penton or hexon (Fig. 5e, g). N1D10 approaches the DII with an orientation nearly parallel to the viral membrane, and the assembly of peplomers would preclude N1D10 binding (Fig. 5e, h). Viral breathing or dynamic motions have been reported for different kinds of viruses, and SFTSV might share similar strategies for cryptic epitope exposure, explaining why B1G11 still had moderate neutralization activity.

S2A5 binds to the top side of the authentic SFTSV virion with an orientation nearly perpendicular to the viral membrane (Fig. 5b, e), and two distinct binding states were observed. In some environments, the binding of S2A5 to reference Gn of the averaged SFTSV virion may

https://doi.org/10.1038/s41467-024-51108-z

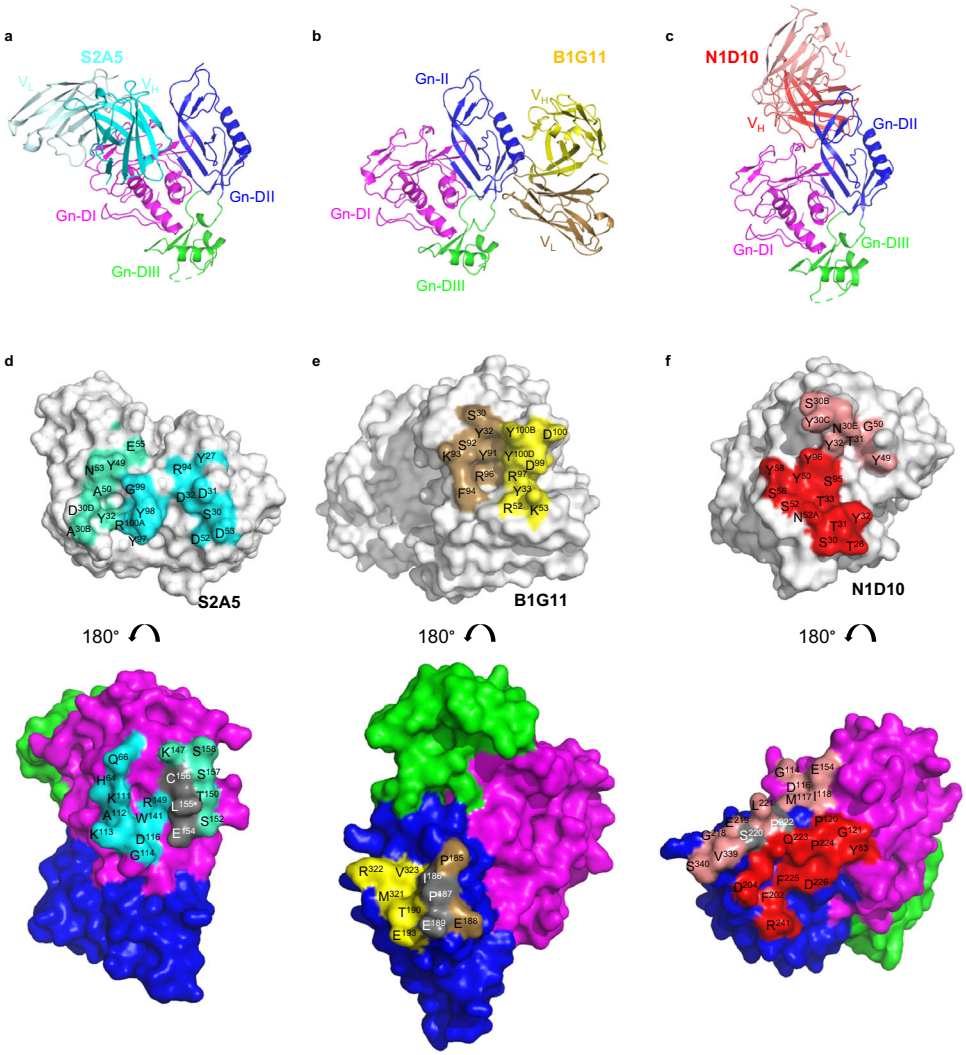

Fig. 4 | Molecular determinants of three Gn mAbs. a–c Ribbon diagrams of Gn head domain complexed with antibody. For clarity, the constant domains of Fab were not displayed. The heavy chain and light chain variable domains of S2A5, B1G11, and N1D10 are shown in cyan and pale cyan, yellow and sand, red and salmon, respectively. Gn is colored by domains: DI, magenta; DII, blue; DIII, green. **d–f** Surface representation of mAb (top) and Gn head (bottom) with contacts labeled and colored as in (**a**). Gn residues contacted by both chains are colored gray.

cause a slight clash with DIII from the adjacent Gn protomer, and the flexible loops from DIII of Gn and CDR-L1 of DIII need to adjust to accommodate the interaction. In another conditions, outside of the primary binding sites of reference Gn, S2A5 likely employs its CDR-L1 to bind DIII from neighboring Gn molecules (Fig. 5f), which raises the possibility of spanning two Gn proteins on the viral surface.

To validate this hypothesis, we generated 3 light chain mutant mAbs comprising alanine substitution in light chain regions of 26–30C (S2A5-L1^{A}), 66-69 (S2A5-L2^{A}), and 91-92 (S2A5-L3^{A}) which presumably affects the interaction with adjacent Gn molecule, and 2 heavy chain mutant mAbs in CDR-H1 (S2A5-H1^{A}: D31A and D32A) and CDR-H3 (S2A5-H2^{A}: Y98A and R[100A]A) which are expected to disrupt the binding to the primary Gn protomer. The binding affinity to recombinant Gn head domain and neutralization activities of WT and mutant S2A5 mAbs to the authentic SFTSV were investigated (Supplementary Fig. 6). Binding affinity of S2A5-H1^{A} and S2A5-H2^{A} to purified Gn head protein decreased more than 2500-fold, and the two mutants had no/poorly inhibitory activities against authentic SFTSV QD02 and WCH97, which suggests that the binding of S2A5 to the authentic SFTSV virion is dominantly controlled by the reference Gn. S2A5-L2^{A} and S2A5-L3^{A} lost ~5-fold binding ability, and they displayed 8- to 23-fold lower inhibitory activity against two authentic SFTSV strains infection than the WT S2A5. S2A5-L1^{A} reduced ~11-fold binding affinity to Gn head protein (Supplementary Fig. 6a), whereas its neutralizing potency against authentic SFTSV viruses decreased by >600-fold (QD02) or 69-fold (WCH97) compared to the WT S2A5 (Supplementary Fig. 6b, c). These data indicate that the CDR-L1 of the light chain likely makes contacts with the neighboring Gn, and the cross-linking of two Gn protomers on the virion surface plays an important role in the neutralizing potency of S2A5.

S2A5 protects mice from lethal SFTSV challenge

To determine whether neutralizing mAbs protect against SFTSV infection in vivo, we first investigated the prophylactic efficacy of two mAbs with distinct and novel epitopes in IFN-α/β receptor knockout (IFN-α/βR-) mice against a more pathogenic authentic SFTSV (strain HBMC5, genotype D virus) infection. In this setting, 6- to 8-week IFN-α/βR-mice ($n = 6$) received a single 400 μg dose of anti-Gn or isotype control mAbs via the intraperitoneal route (i.p.) 24 h before SFTSV inoculation (Fig. 6a). Treatment of mice with modest neutralizing mAb (B1G11) or non-binding isotype control mAb (NiV E2) failed to protect mice from infection with significant weight loss, ruffled fur, and depression from 2 days post-infection (dpi), and all mice succumbed to infection by 5-8 dpi. Mice treated with S2A5 were completely

https://doi.org/10.1038/s41467-024-51108-z

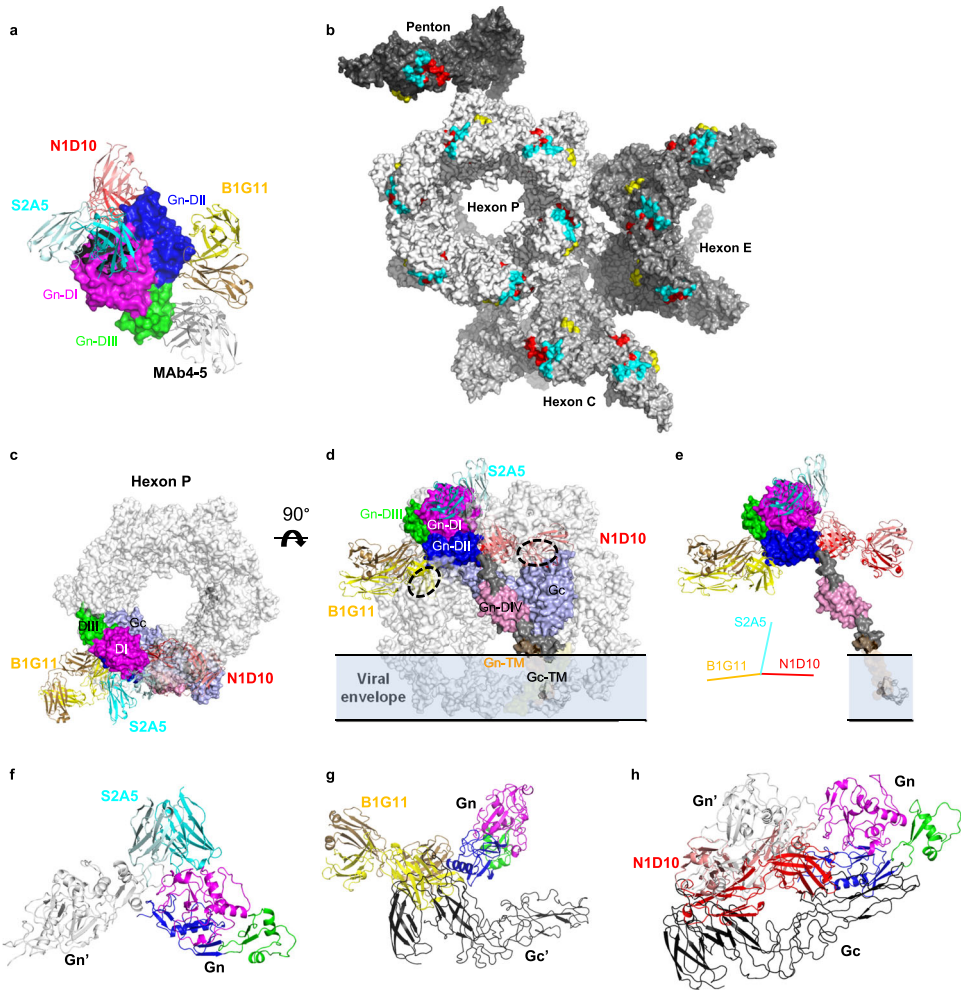

Fig. 5 | Accessibility of Gn epitopes on SFTSV virion. a Superimposition of the S2A5-Gn, B1G11-Gn, N1D10-Gn, and MAb4-5-Gn (PDB: 5Y11) complexes onto Gn head domain. MAbs S2A5, B1G11, and N1D10 are colored cyan, yellow, and red, respectively. **b** Epitope mapping within an asymmetric unit (ASU) of the SFTSV virion (PDB:8I4T). The epitopes of S2A5, B1G11, and N1D10 on virion are highlighted in cyan, yellow, and red, respectively. **c**, **d** Docking of the S2A5, B1G11, and N1D10 Fabs onto the hexon peplomer (hexon P) of the SFTSV virion. **c** Top view of the hexon peplomer. **d** Side view of the hexon peplomer. The Gn from reference Gn/Gc heterodimer is colored by domains (DI: magenta; DII: blue; DIII: green; domain IV: pink; linker: grey50; transmembrane domain (TM): orange). The ectodomain of Gc from reference Gn/Gc is colored sky blue, linker is colored grey50, and TM is colored olive. The other five subunits are colored white. Clashes with adjacent Gn or Gc molecules were indicated with a black circle. **e** Comparison of the orientations of mAbs relative to the viral membrane. **f-h** Close-up views of interaction/clashes between S2A5 and adjacent Gn molecule (**f**), B1G11 and adjacent Gc molecule (**g**), N1D10 and adjacent Gn/Gc heterodimer (**h**). The neighboring Gn molecule is colored white, and Gc is colored black.

protected against SFTSV infection without weight loss during 15 days of observation (Fig. 6c). These results indicate that the strength of neutralizing activity of anti-Gn mAbs in vitro is a critical factor for SFTSV in vivo protective effect against SFTSV challenge.

As S2A5 has great protective activity against SFTSV infection as prophylaxis, we next examined the therapeutic efficacy of this mAb. IFN-α/βR-mice were intraperitoneally challenged with SFTSV (500 $TCID_{50}$) and then a single dose of S2A5 was administered by i.p at 6, 24, or 48 h post-infection (hpi) (Fig. 6b). For the isotype control mAb-treated group, all mice died within 6 days. For S2A5-treated groups, the mice injected with a single dose of S2A5 at 6 hpi exhibited a 100% survival rate, and consistent body weight increases were observed over the course of the experiment. All mice administered S2A5 at 24 hpi survived, although the weight loss was observed within 6 days after infection. We also observed 33% survival of mice treated with S2A5 at 48 hpi (Fig. 6d). In addition, treatment with S2A5 at 6 hpi or 24 hpi remarkably reduced viral loads in serum, liver and spleen tissues (Fig. 6e–g). SFTSV infection led to decreased platelet counts in the peripheral blood of the control group; however, no significant platelet count decrease was detected in the S2A5-treated groups, further supporting the therapeutic efficacy of the antibody (Fig. 6h). Similar results could be observed in white blood cell (WBC) counting analyses, although no statistical significance was obtained probably due to individual differences in the disease progression (Fig. 6i). Consistently, treatments with S2A5 also seemed to alleviate the increase of serum alanine aminotransferase (ALT) and aspartate aminotransferase (AST) concentrations (markers for organ injury) (Fig. 6j, k). Taken together, these results indicate that a single dose of S2A5 administration could efficiently protect IFN-α/βR-mice from lethal SFTSV infection in both pre- and post-exposure treatments. This result also emphasizes the importance of the dosing window after SFTSV infection, and S2A5 treatment within 48 h can assist the mice in reducing virus infection to varying degrees.

Discussion

There is a pressing need to develop antivirals against SFTSV infection. Here, we isolated a panel of SFTSV Gn-specific mAbs and revealed three novel epitopes of these mAbs with varying inhibitory activities. Mechanistically, the most potent mAbs targeting the DI of Gn work at both viral attachment and fusion steps, whereas the less potently

https://doi.org/10.1038/s41467-024-51108-z

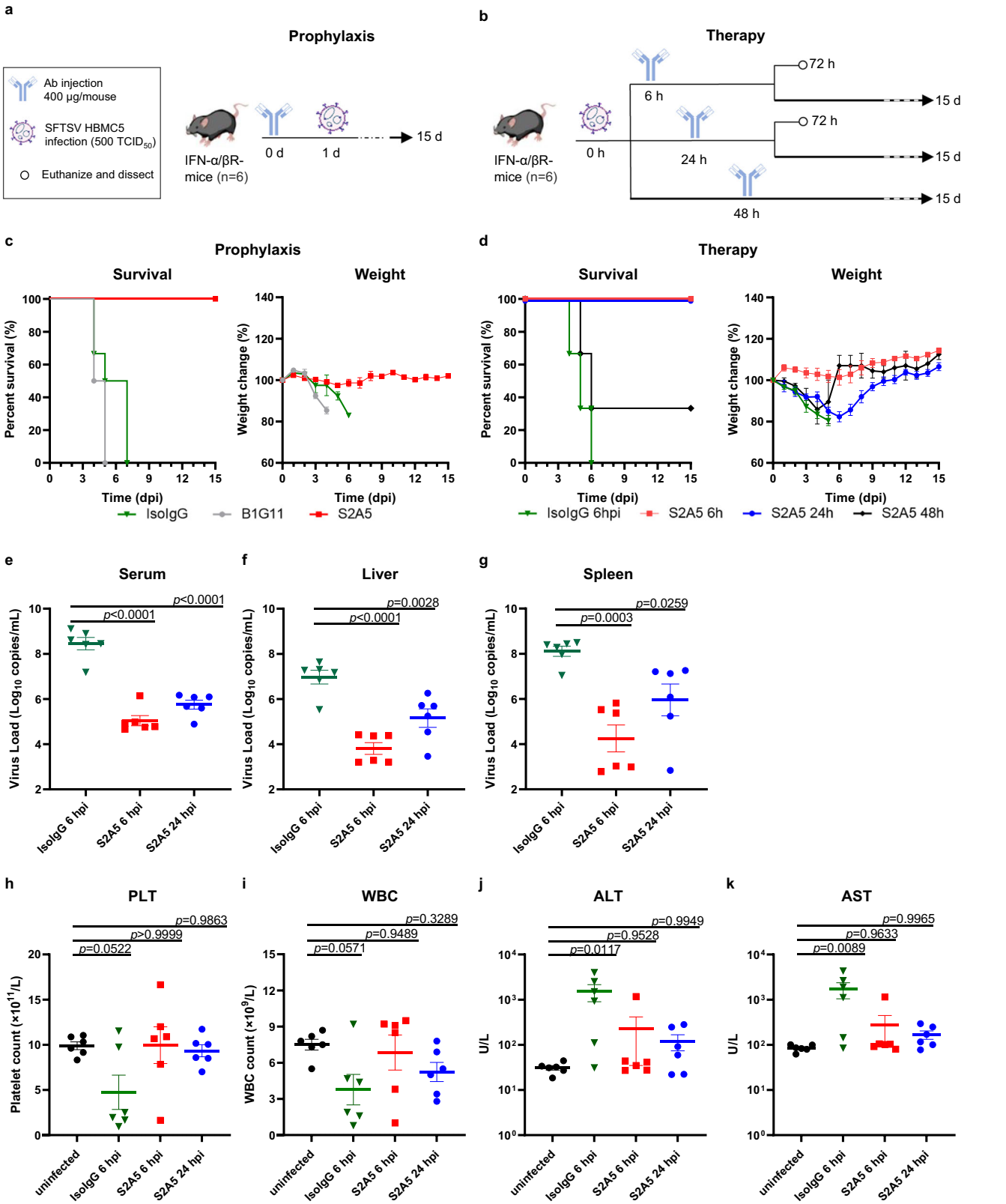

Fig. 6 | S2A5 protects mice from lethal SFTSV challenge. a, **b** In vivo prophylactic (**a**) or therapeutic (**b**) treatment regimen. **c** Mice (n = 6) were administered with indicated antibodies via an intraperitoneal route (i.p.); 24 h later, the treated mice were intraperitoneally infected with the SFTSV HBMC5 strain. Then, weight and survival rate of mice were continuously monitored for 15 days. **d** Mice ($n = 6$) were intraperitoneally infected with SFTSV HBMC5 strain first, then the infected mice were injected with indicated antibodies (i.p.) 6, 24, and 48 h post-infection. Weight data represent mean ± SEM of mice remaining at each time point. **e**–**k** The experiments were performed as (**b**), except that mice ($n = 6$) were sacrificed on the third day of infection for analyses of the viral loads in different tissue samples (**e**–**g**) and blood routine and biochemical indexes (**h**-**k**). Each data point represents an individual mouse within the respective groups. Isotyped IgG, IsoIgG; platelet, PLT; white blood cells, WBC; indicators for organ (liver) injury: serum aspartate aminotransferase (AST) and alanine aminotransferase (ALT). The data were subjected to one-way ANOVA with Dunnett's test in the comparison to IsoIgG treated group. Bars show mean ± SEM, revealing a significant difference with $p < 0.0001$ (****), $p < 0.001$ (***), $p < 0.01$ (**), $p < 0.05$(*). Source data are provided as a Source data file.

neutralizing mAbs recognizing Gn DII (B1G11) can only partially inhibit virus binding to the cells. Importantly, one of the DI mAbs (S2A5) likely cross-links two Gn subunits on the SFTSV virion and provides both pre- and post-exposure protections against SFTSV infection in vivo. This work maps the antigenic determinants of Gn and underscores that Gn DI is a potential target for protective mAb development.

Previous study has shown that fatal SFTSV infection can disrupt humoral immunity and antibody response[35]. In addition, the number of SFTSV-protective human mAbs is relatively smaller than other bunyaviruses or pathogenic viruses. To study the immunogenicity of SFTSV and develop the potential anti-SFTSV mAbs, we immunized mice with different antigens and strategies, and isolated seven Gn-specific mAbs. We originally immunized BALB/c mice with recombinant Gn head domain and found that the neutralizing titers of the serum against two SFTSV pseudotyped viruses varied across immunized mice. Then, we immunized mice with infectious chimeric rVSV-eGFP-SFTSV, which induced much higher neutralizing titers at polyclonal serum level than mice injected with purified Gn head protein (Supplementary Fig. 1). Despite different neutralizing titers at polyclonal serum levels, we obtained potently neutralizing mAbs from both protein-immunized and chimeric rVSV-eGFP-SFTSV-immunized mice (Supplementary Table 5).

MAb4-5, isolated from the human antibody library that targets the DIII of Gn, is the only SFTSV-neutralizing antibody with a structurally defined epitope[20]. In our panel, S1H7 recognizes a competitive epitope with MAb4-5. Interestingly, S1H7 displayed comparable or slightly better inhibitory activity than MAb4-5 against pseudotyped and authentic SFTSV, suggesting that the epitope shared by MAb4-5 and S1H7 is immunogenic in humans and mice (Table 1). An alanine substitution analysis mapped the binding footprint of a human mAb Ab10 to the residues within DII, which is also the domain targeted by B1G11. Comparing the Gn residues engaged by B1G11 and Ab10, only residues R322 and V323 are shared contacts by the two mAbs, and other interacting residues are unique contacts for each mAb, which likely explains the distinct protection capacity of B1G11 and Ab10[26]. Notably, we also discovered two cross-reactive mAbs (S1E9 and N1D10), which recognize the Gn proteins of SFTSV, HRTV, and GTV. S1E9 and N1D10 are derived from distinct B cell germlines (Supplementary Table 5), but they are grouped into the same class based on the competition BLI assay and exhibit similar cross-reactivity profiles. Structural analysis of N1D10 in complexed with Gn defines a relatively conserved non-neutralizing epitope on the Gn, which likely evolves slowly over SFTSV and its closely related pathogens.

B1G11, with modest neutralizing capacity, shows the highest binding affinity to recombinant Gn protein, which is around 10- to 70-fold higher than the most potently neutralizing antibodies S2A5, S1G3, and S1H7 (Fig. 2b, Table 1 and Supplementary Table 6). Structural and epitope mapping studies show that they target three distinct epitopes on Gn. B1G11 recognizes the DII of Gn, S2A5 targets the DI of Gn, and S1H7 binds to a non-overlapping antigenic region with B1G11 and S2A5 (Fig. 2a and Fig. 5). These results suggest that the epitopes targeted by the mAbs are more critical for the function than the binding affinity to the recombinant protein. We and others have shown that the same germline genes-derived mAbs usually exhibit similar binding profiles[36–40]. As S2A5 and S1G3 are derived from same V, D, J fragments of heavy chain and V, J fragments of light chain (Supplementary Table 5), we believe that S2A5 and S1G3 are sibling clones and should have almost identical binding footprints and interaction modes on Gn. As expected, S2A5 and S1G3 are grouped into the same class based on the competition-binding and Gn mutation studies, and they possess strong inhibitory activity against tested SFTSV strains. However, S2A5 showed slightly better neutralizing efficacy than S1G3, likely due to the binding affinity, as K_D values of S2A5 are ~10-fold lower than that of S1G3.

Two recent studies reported that SFTSV Gn-specific mAbs (Ab10 and SNB02) could protect mice from SFTSV infection[26,28]. However, multi-dose injections of mAbs (four times treatment with 400 μg/mice for SNB02 and four times treatment with 600 μg per mouse for Ab10) were used in these studies. We observed protective efficacy for the most potent mAb S2A5 in both pre- and post-exposure settings with a single injection at a lower dose (400 μg per mouse). S2A5 exhibits potent inhibition against six SFTSV pseudotyped viruses, representing all reported genotypes of SFTSV (genotypes A-F). Consistently, it strongly neutralizes authentic SFTSV genotypes A and D strains with IC_{50} values less than 40.2 ng/mL (Fig. 1 and Table 1). The complex structure of S2A5 Fab with Gn head shows that the binding epitope of S2A5 on the Gn is highly conserved across all six SFTSV genotypes, corroborating the pseudotyped SFTSV neutralization results. These results support that S2A5 is a broadly neutralizing and protective SFTSV mAb, which could be considered a candidate for the prophylaxis and therapy of SFTSV infection in the future.

Although attachment blocking is a classical neutralization mechanism adopted by potent mAbs, accumulated data have shown that viral fusion blockade is an extremely important and alternative inhibitory mechanism used by potent mAbs. Other related bunyavirus studies have reported that human mAbs against Sin Nombre virus (mAb SNV-42) and Rift Valley Fever virus (group A2 mAbs) recognize the antigenic sites of Gn and interfere fusion step[41,42], which is similar to the most potent mAbs (S2A5, S1G3, and S1H7) in our panel. Epitope mapping indicated that SNV-42 targets the DIII of Gn, and the anti-RVFV group A2 mAbs predominantly recognize the DI of Gn. We showed that the two DI mAbs (S2A5 and S1G3) and group C mAb S1H7 (competing with DIII mAb MAb4-5) exhibit attachment and fusion inhibition capacities. Taken together, these results suggest that the neutralizing mAbs against the DI and DIII of Gn can inhibit bunyavirus infection through a fusion blockade mechanism, likely by disturbing the glycoproteins transition necessary for fusion.

In summary, we isolated and characterized a panel of SFTSV-Gn mAbs. Structural and epitope-binning studies uncover four distinct antigenic determinants on the SFTSV Gn, covering all three domains of Gn head. Three epitopes have not been identified before and targeted by mAbs with gradient neutralizing capacities. The potently neutralizing mAb S2A5 in our panel is highly protective against severe disease and death caused by SFTSV infection in vivo and works by inhibiting both viral attachment and fusion steps. Overall, this study provides potential antiviral reagents for prophylaxis and therapy against SFTSV infection and may guide the vaccine design against SFTSV and other bunyaviruses.

Methods

Ethics statement

The mice immunization experiments were approved by the Animal Care and Use Committee of Wuhan University (Approval: WDSKY0202201 and SKLV-AE2023 025). The mice passive protection experiments were approved by the Biosafety Committee and the Animal Ethical Committee of Wuhan Institute of Virology, Chinese Academy of Sciences (WIV, CAS. Approval: WIVA23202302) and were conducted at the Central Animal Laboratory of Wuhan Institute of Virology. Every attempt was made to minimize potential suffering and reduce the number of animals used in the research, following institutional guidelines.

Viruses and cells

The SFTSV strain QD02 (GenBank accession number: MW526369.1) was generously provided by Dr. Xue-jie Yu from Wuhan University. SFTSV strains WCH97 (GenBank accession number: JQ341189.1) and HBMC5 (GenBank accession number: KY440770.1) were preserved in the National Virus Resource Center (NVRC, Wuhan, China). All authentic viruses were propagated and titrated in Vero E6 cells. Vero

E6 or 293T cells were maintained in DMEM (Monad) supplemented with 8% or 10% heat-inactivated FBS (ExCell Bio) at 37 °C with 5% CO_2.

Plasmids

The coding region of SFTSV Gn head domain (residues 20-340, GenBank: JQ341189.1, genotype A strain) was cloned into the baculovirus-insect expression vector pFastBac1, as well as a mammalian expression vector with a C-terminal 6×His-tag. HRTV Gn head domain (residues 22–342, GenBank: LC629154.1), GTV Gn head domain (residues 19-337, GenBank: KT328592.1) and SFTSV Gc (residues 562-996, GenBank: JQ341189.1) were individually cloned into the mammalian expression vector with a C-terminal 6×His-tag. The Gn mutants were generated by site-directed mutagenesis.

The M segment (residues 1-1073) of six SFTSV genotypes was cloned into the pCAGGS vector for VSV-based pseudovirus generation. The M coding regions of strains QD02 (genotype D, GenBank: MW526369.1)[43] and WCH97 (genotype A, GenBank: JQ341189.1) were amplified from the virus cDNA. The M of SFTSV strains KAGBH5 (genotype B, GenBank: KP663738.1), AHL/China/2011 (genotype C, GenBank: JQ670930.1), SD4 (genotype E, GenBank: HM802203.1) and HNXY_186 (genotype F, GenBank: KC292308.1) were obtained through point mutation using the SFTSV QD02 or WCH97 M genes as templates.

Protein expression and purification

The SFTSV Gn head domain protein was produced using the Bac-to-Bac baculovirus expression system. In summary, purified recombinant bacmids were transfected into sf9 cells by FuGENE 6 Transfection Reagent (Promega) to generate baculovirus. This stock was then used to infect Hi5 cells to express Gn protein. The GTV and HRTV Gn proteins were obtained through a mammalian cell expression system by transfecting Expi293 cells with GTV/HRTV Gn protein expression vectors using Polyethylenimine (PEI, Polysciences). SFTSV/GTV/HRTV Gn proteins in the supernatant were collected and purified using Ni-Charged Resin (GenScript). Further purification of Gn proteins was performed with a Superdex 200 increase column (Cytiva) in a buffer containing 20 mM Tris-HCl pH 8.0 and 150 mM NaCl.

SFTSV pseudovirus production

VSV-based SFTSV M pseudotyped viruses (single replication cycle) were generated according to previously published protocols[44,45]. Briefly, 293T cells were transfected with plasmids containing the M gene of different SFTSV genotypes (A-F) using GeneTwin reagent (Biomed). After 24 h, the transfected cells were exposed to VSV-dG-eGFP (1×10^6 FFU) diluted in DMEM with 4% FBS for 6 h at 37 °C. The cells were washed and replenished with fresh medium (DMEM with 4% FBS) containing anti-VSV-G monoclonal antibody (mAb I1, diluted at 1 μg/mL)[46]. After an additional 24 h of culture, the supernatant containing the SFTSV pseudovirus was harvested, aliquoted, and stored at −80 °C.

Replication-competent chimeric VSV containing SFTSV M genes (rVSV-eGFP-SFTSV) was generated and amplified as described previously[47]. Briefly, 293T cells were infected with vaccinia virus vTF7-3, which expresses T7 RNA polymerase, and subsequently co-transfected with plasmids individually expressing VSV N, P, G, L, and the viral genome (containing VSV N, P, M, L, and SFTSV M in one vector) under the control of T7 promoter. 48 h post-transfection, the supernatants were centrifugated at 3,000 *g* for 10 min, filtered through a 0.22 μm filter, and collected as passage 0 (P0) virus stock. For passage 1 (P1) virus amplification, Vero E6 cells were transfected with a VSV G-expressing vector and then infected with above P0 virus. The infected cell supernatants (P1 virus) were collected and filtered through 0.45 μm filters when an apparent cytopathic effect (CPE) was observed. The P1 virus was then inoculated into Vero E6 cells to make VSV-based infectious SFTSV stocks (rVSV-eGFP-SFTSV). The functional titer of the chimeric rVSV-eGFP-SFTSV was determined based on the GFP signal using a serial dilution-based infection assay on Vero E6 cells.

Mouse immunization and cell sorting

BALB/c mice were intraperitoneally injected with 10^6 FFU of infectious chimeric rVSV-eGFP-SFTSV three times or intramuscularly injected four times with 10 μg of SFTSV Gn protein emulsified with the adjuvant AddaVax (InvivoGen). Then, the mice were euthanized on day 5 after the final boost with 25 μg of SFTSV Gn protein (12.5 μg intravenously and 12.5 μg intraperitoneally), and the spleens were isolated for cell sorting as previously reported[48]. Briefly, SFTSV Gn protein was randomly biotin-labeled (biotin-Gn) using EZ-Link-NHS-PEG4-Biotin (Thermo Fisher) according to the manufacturer's protocol, then the excess biotin was removed by passing the sample through a desalting column (Thermo Fisher). The mice splenocytes were harvested to make single-cell suspensions, then the cells were incubated with biotin-Gn at 0.5 μg/mL for 30 min, followed by the staining with anti-CD19, anti-CD3/4/8, anti-IgD, anti-CD95, anti-CD38, and Streptavidin-APC. Antigen-specific plasma B cells ($CD19^+CD3/4/8^-IgD^-CD95^+APC^+$) were sorted into 96-well plates with one cell per well using FACS Aria III flow cytometer (BD Biosciences).

MAb generation

The variable region sequences of paired mAbs were determined using previously reported protocols with minor modifications[48,49]. Briefly, complementary DNA was produced using the HiScript II 1st Strand cDNA Synthesis Kit (Vazyme), followed by amplifying V_H and V_L genes using first-round and nested primer sets. Subsequently, the PCR products were analyzed on 1% agarose gels, and approximately 400 bp DNA bands were extracted and sequenced. To generate recombinant antibodies, the V_H and V_L segments were PCR-amplified from first-round PCR products and then individually cloned into AbVec2.0-IGHG1 (Addgene) and AbVec1.1-IgKC (Addgene) expressing vectors. The V_H segments were also subcloned into a modified AbVec2.0-IGHG1 vector with a C-terminal 6×His-tag terminating after the CH1 constant region for Fab expression. The paired heavy and light-chain expression plasmids of the mAbs or Fabs were co-transfected into Expi293 cells using PEI. 6 days post-transfection, cell supernatants containing monoclonal antibodies or Fabs were collected and purified using rProtein A resin (Smart-Lifesciences) or Ni-Charged Resin (GenScript). The purified mAbs were buffer-exchanged into PBS, and Fabs were further purified through size-exclusion chromatography (SEC) with a Superdex 200 increase column (Cytiva) in 20 mM Tris-HCl pH 8.0 and 150 mM NaCl.

Enzyme-linked immunosorbent assay (ELISA)

Purified proteins were immobilized onto 96-well plates (96-Well High-Binding Flat-Bottom Microplate, Corning) in a carbonate buffer (200 ng per well) and incubated at 4 °C overnight. For authentic SFTSV virons detection, virus QD02 were immobilized onto 96-well plates at 37 °C for 1 h, and cell culture supernatant (without viral infection) was simultaneously immobilized to eliminate interference from non-specific binding caused by cellular metabolites or debris. After three times washing with PBST (PBS with 0.05% Tween 20), blocking was performed using 1% BSA in PBST. Subsequently, a diluted antibody was added and incubated at room temperature for 1 h. Following three times washing, the HRP conjugated goat anti-human IgG (H + L) (1:10,000, ABclonal), diluted in PBST with 1% BSA was added and incubated for an additional hour. After three times washing, the TMB (3,3′,5,5′-tetramethylbenzidine) substrate was applied, and the reaction was stopped by adding 1 M HCl. Absorbance at 450 nm was measured and recorded. The obtained data were analyzed using GraphPad Prism 9.

Focus forming and reduction neutralizing assay

Virus titration was determined using a focus-forming assay (FFA). In brief, Vero E6 cell monolayers were inoculated with either the virus or a virus-mAb mixture (pre-incubated at 37 °C for 1 h). After 1 h of incubation in a 37 °C incubator, cells were washed and cultured in DMEM supplemented with 2% FBS. After 36 h, cells were fixed with 4% paraformaldehyde (PFA), followed by a 20 min incubation with 0.5% Triton X-100 diluted in PBS. Subsequently, cells were blocked with 1% BSA (diluted in PBS) for 1 h, and an anti-SFTSV-Gn antibody (MAb4-5, with 1% BSA diluted in PBS)[20] was added overnight at 4 °C. Then, cells were washed three times with PBS, and Alexa Fluor 488 anti-human IgG antibody (Invitrogen), diluted in PBS at a volume ratio of 1:1000, was added and incubated for 1 h at room temperature. After washing, virus-infected foci were observed, and a 50% tissue culture infective dose ($TCID_{50}$) was calculated using the Reed-Muench method[50].

Focus reduction neutralization tests (FRNT) were conducted using indicated authentic SFTSV strains or pseudoviruses with mAbs in Vero E6 cells in a 96-well plate, following a previously described protocol[36]. The infection frequency of wells inoculated with the virus in the presence of mAb was compared with that of wells inoculated with the virus alone. The virus-infected foci were counted using the ImmunoSpot 5.0.37 macroanalyzer (Cellular Technologies), Celigo Image Cytometer (Revvity, Lawrence, MA) or the Operetta CLSTM high-throughput system (PerkinElmer, Waltham, MA, USA). The half-maximal inhibition concentration (IC_{50}) was determined using non-linear regression analysis with GraphPad Prism.

Biolayer interferometry assay (BLI)

For the evaluation of binding affinity, purified mAb was immobilized onto a protein A biosensor (ForteBio), then the biosensors were dipped into wells containing serially diluted Gn proteins. All proteins were diluted in a neutral running buffer (10 mM HEPES pH 7.4, 150 mM NaCl, 3 mM EDTA, and 1% BSA) or in an acid buffer (10 mM HEPES pH 5.0, 150 mM NaCl, 3 mM EDTA, and 1% BSA), and 10 mM glycine (pH 2.0) was employed to regenerate the biosensors. The experiment was conducted at 25 °C. Sensors without antibody loading were used in parallel to establish the background, and the binding and dissociation values were analyzed using Octet data analysis software (version 12.2.0.20).

The competition-binding relationships were investigated using a competitive BLI assay. In this assay, the first mAb was initially loaded onto protein A biosensors and then associated with Gn protein. Subsequently, the biosensors were immersed into the buffer containing the same first or tested mAbs (10 μg/mL) for 300 s. The increased binding signal of the second mAb to the first mAb captured Gn was calculated and expressed as a percentage binding over the non-competitor second mAb (maximal binding). The antibodies were defined as a strong competitive group if the percentage binding signal was less than 25%.

SFTSV Gn-Fab complexes crystallization and structure determination

Purified B1G11, S2A5, or N1D10 Fab was individually mixed with the purified SFTSV Gn protein with a molar ratio of 1.2:1. Fab-Gn complex was isolated by size exclusion chromatography using a Superdex 200 10/300 Increase column in 20 mM Tris-HCl pH 8.0 and 150 mM NaCl. Crystallization of Fab-Gn complex was performed by sitting drop vapor diffusion at 16 °C. Typically, 8 or 10 mg/mL Fab-Gn complex was mixed with the precipitant/reservoir solution at a 1:1 volume ratio in a 0.6 μL drop. For the B1G11 Fab-Gn complex, crystals grew in a precipitant solution containing 0.1 M HEPES pH 6.5 and 20 % wt/vol Jeffamine ED2003. For the S2A5 Fab-Gn complex, crystals were obtained in the condition of 0.1 M HEPES pH 7.0, 40% vol/vol pentaerythritol propoxylate (5/4 PO/OH), and 0.2 M sodium thiocyanate. For the N1D10 Fab-Gn complex, crystals were obtained in the condition of 0.095 M Tri-sodium citrate pH 5.6, 19% (vol/vol) isopropanol, 19% (wt/vol) PEG 4000, and 5% (vol/vol) glycerol. Crystals were stepwise transferred to a cryostabilizer solution (precipitant solution supplemented with 15-20% [vol/vol] glycerol) and then flash-cooled in liquid nitrogen before data collection.

The X-ray diffraction data were collected at the BL02U1 or BL10U2 beamline of the Shanghai Synchrotron Radiation Facility (SSRF) with a wavelength of 0.9792 Å and a temperature of 100 K. A total of 360 degrees of data were collected in 0.2 to 0.4° oscillation steps. The diffraction data were automatically processed by the pipeline Xia2[51], XDS[52], and DIALS[53] at the beamlines and scaled with Aimless[54] in the CCP4 suite[55]. Phasing was obtained by molecular replacement using PHASER[56] with the previously reported SFTSV Gn structure (PDB code: 5Y10) and the predicted Fab structures by AlphaFold2[57] as search models. Iterative model building and refinement were performed using Coot[58] and PHENIX[59]. The data collection and refinement statistics for the final models are listed in Supplementary Table 1.

Flow cytometry

293T cells transiently transfected with Gn, Gc, or Gn mutant plasmids were employed for the binding test. 48 h post-transfection, cells were harvested and fixed with 4% PFA. Cells were then washed and permeabilized with PBS supplemented with 0.1% saponin, followed by the staining with indicated SFTSV mAbs in permeabilization buffer at 4 μg/mL. After washing twice, the cells were incubated with Alexa Fluor 488 anti-human IgG antibody (Invitrogen). Then, the cells were rewashed and subjected to analysis using a CytoFLEX S (Backman). Wild-type Gn and Gc expression plasmids were included as positive and negative controls. Residues were considered critical if the binding level decreased >70% compared to the wild-type Gn.

Fusion inhibition assay

The SFTSV M-mediated cell-cell fusion was induced by low pH condition and cell fusogenicity were measured by a dual-split-reporter (DSP, renilla luciferase [Luc] and green fluorescent protein [GFP]) system described previously[45,60]. Briefly, two groups of 293T cells were prepared, then group A cells were transfected with 1.5 μg SFTSV M plasmid and 1.5 μg reporter plasmid A (DSP1-7), and group B cells were co-transfected with 1.5 μg SFTSV M plasmid and 1.5 μg reporter plasmid B (DSP8-11). The two group cells were cultured for 24 h, detached, mixed (1:1) and replaced in 96-well plate. The mixed cells were cultured for additional 24 h and then supernatant was replaced with fresh DMEM containing indicated mAbs. 2 h later, cells were washed with DMEM to remove unbound mAbs and then treated with 0.1 M citrate pH 5.0 for 5 min at room temperature to induce M-mediated cell-cell fusion. After this, the acidic medium was replaced with fresh DMEM supplemented with 4% FBS and 10 mM HEPES (pH 7.4) and cells were incubated at 37 °C for 24 h, then fluorescent images were captured using a Celigo Image Cytometer (Revvity, Lawrence, MA) to monitor GFP-positive cells. For live-cell luciferase activity measurements, 20 μM of EnduRen live-cell substrate (Promega, E6481) was diluted in DMEM and added to the cells. The cells were then incubated for at least 1 h before detection using the Varioskan LUX Multi-well Luminometer (Thermo Fisher Scientific). The luciferase activity measurement in the sample without the addition of mAb was used to define 100% fusion and calculate the membrane fusion percentage for each mAb treatment.

Quantitative reverse transcription PCR (qRT-PCR)

Attachment blockade was assessed by quantitative reverse transcription-polymerase chain reaction (qRT-PCR) on a CFX connected real-time PCR system (Bio-Rad). Briefly, SFTSV (10^4 $TCID_{50}$) was pre-incubated with mAb (10 μg/mL, 100 μg/mL) for 30 min. Then, the mixture was added to 24-well plates with chilled Vero E6 cells for 30 min at

4 °C. After three times washing with cold PBS on ice, 0.5 mL Trizol (Thermo Fisher) was added to each well. Total RNA was extracted as described before, and SFTSV RNA levels were determined using the ChamQ SYBR qPCR Master Mix Kit (Vazyme), normalized to the internal control GAPDH. The primer sequences used are as follows: SFTSV-L-Fwd, 5′- AGTCTAGGTCATCTGATCCGTTYAG-3′; SFTSV-L-Rev, 5′- TGTA AGTTCGCCCTTTGTCCAT-3′; GAPDH-Fwd, 5′- ATGGGGAAGGTGAAGGT CGG-3′; GAPDH-Rev, 5′- TTACTCCTTGGAGGCCATGTG-3′[61].

The virus RNA from frozen serum (50 µL) and tissues (10 mg) of mice was extracted using a mini viral RNA extraction kit (Takara, 9766) and quantified by qRT-PCR using the following primers and probe: SFTSV S segment (forward: GGGTCCCTGAAGGAGTTATAAA; reverse: TGCCTTCACCAAGACTATCAATGT; probe: TTCTGTCTTGCTGGCTCC GCGC).

Pre- and post-attachment neutralization assays

For the pre-attachment inhibition assay, 10^4 $TCID_{50}$ of SFTSV was mixed with serial dilutions of mAbs and incubated for 1 h at 4 °C. The virus-mAb mixture was then inoculated onto chilled Vero E6 cells for 1 h. Following the incubation, the cells were washed three times with cold PBS to remove unbound virus and replenished with fresh DMEM (2% FBS). Subsequently, the plates were transferred to a 37 °C incubator, and standard FRNT was performed as described above.

For post-attachment inhibition detection, chilled Vero E6 cells were initially inoculated with 10^5 $TCID_{50}$ of SFTSV. After 1 h of incubation at 4 °C, the cells were washed with cold PBS to remove extra virus, and serial dilutions of mAbs were added to each well on ice. The cells were then incubated at 4 °C for one hour, followed by extensive washing to remove unbound mAbs. Standard FRNT was subsequently conducted as described above.

Passive protection against SFTSV HBMC5 strain challenge in mice

The IFN-α/β receptor knockout mice (B6.129S2-*Ifnar1*^{tm1Agt}/Mmjax, RRID: MMRRC_032045-JAX), which were generated by Müller et al[62], were kindly provided by Dr. Leike Zhang (WIV, CAS), and were bred and maintained under specific pathogen-free conditions. 6- to 8-week-old female IFN-α/β receptor knockout mice were randomly assigned to groups (n = 6). For the prophylactic study, the mice were intraperitoneally administered mAb S2A5 or B1G11 (400 µg each mouse) or isotype control mAb (NiV E2, anti-NiV mAb without binding to SFTSV) 24 h before intraperitoneal challenge with 500 $TCID_{50}$ SFTSV (strain HBMC5). For the post-exposure treatment, the mice (n = 6) were first anesthetized and intraperitoneally inoculated with 500 $TCID_{50}$ of SFTSV, and 6, 24, or 48 h post-infection (hpi), the infected mice were passively injected with S2A5 (400 µg each mouse), and the control group was given isotype control mAb NiV E2 with the same dose at 6 hpi. In the prophylactic or therapeutic study, each mouse was examined daily for behavior, body weight, and mortality for 15 days. For the postexposure therapy, we also performed the virological assessment, and mice (n = 6) treated with S2A5 or control mAb were euthanized 3 days post-infection to harvest blood samples, livers, and spleen tissues. White blood cell count (WBC) and platelet count (PLT) in EDTA-treated blood were detected by the auto hematology analyzer (Mindray, BC-2800vet). Blood biochemical indicators, including serum alanine transaminase (ALT) and aspartate aminotransferase (AST) levels in serum, were detected by the automatic biochemical analyzer (Rayto, Chemray-800). Blood counts and biochemical tests from the control group (without infection) were also conducted for reference.

Statistical analysis

All functional results were analyzed using GraphPad Prism (version 9.4.0) software, and differences were evaluated by one-way or two-way ANOVA with Dunnett's multiple comparisons test comparing to the control group (statistical comparison groups are indicated in each of the Figure legends). A p-value of <0.05 was considered significant.

Reporting summary

Further information on research design is available in the Nature Portfolio Reporting Summary linked to this article.

Data availability

All data needed to evaluate the conclusions in the paper are present in the paper or the Supplementary information. Source data are provided with this paper. The atomic coordinates have been deposited to the Protein Data Bank (PDB) with accession codes 8XK5, 8XK6, and 8XK8. The structures are available in the PDB under the following accession codes and links: PDB: 8XK5 https://doi.org/10.2210/pdb8XK5/pdb. PDB: 8XK6 https://doi.org/10.2210/pdb8XK6/pdb. PDB: 8XK8 https://doi.org/10.2210/pdb8XK8/pdb. PDB: 8I4T https://www.rcsb.org/structure/8I4T. PDB: 5Y10 https://www.rcsb.org/structure/5Y10. PDB: 5Y11 https://www.rcsb.org/structure/5Y11 Source data are provided with this paper.

References

1. Yu, X.-J. et al. Fever with thrombocytopenia associated with a novel Bunyavirus in China. *N. Engl. J. Med.* **364**, 1523–1532 (2011).
2. Kuhn, J. H. et al. 2022 taxonomic update of phylum Negarnaviricota (Riboviria: Orthornavirae), including the large orders Bunyavirales and Mononegavirales. *Arch. Virol.* **167**, 2857–2906 (2022).
3. Casel, M. A., Park, S. J. & Choi, Y. K. Severe fever with thrombocytopenia syndrome virus: emerging novel phlebovirus and their control strategy. *Exp. Mol. Med.* **53**, 713–722 (2021).
4. Yang, T., Huang, H., Jiang, L. & Li, J. Overview of the immunological mechanism underlying severe fever with thrombocytopenia syndrome (Review). *Int. J. Mol. Med.* **50**, 118 (2022).
5. Zhang, X. et al. Rapid Spread of Severe Fever with Thrombocytopenia Syndrome Virus by Parthenogenetic Asian Longhorned Ticks. *Emerg Infect Dis* **28**, 363–372 (2022).
6. Egizi, A. et al. First glimpse into the origin and spread of the Asian longhorned tick, Haemaphysalis longicornis, in the United States. *Zoonoses Public Health* **67**, 637–650 (2020).
7. Heath, A. C. G. A history of the introduction, establishment, dispersal and management of Haemaphysalis longicornis Neumann, 1901 (Ixodida: Ixodidae) in New Zealand. *N. Zealand J. Zool.* **47**, 241–271 (2020).
8. Miao, D. et al. Mapping the global potential transmission hotspots for severe fever with thrombocytopenia syndrome by machine learning methods. *Emerg. Microbes Infect.* **9**, 817–826 (2020).
9. Bopp, N. E. et al. Baseline mapping of severe fever with thrombocytopenia syndrome virology, epidemiology and vaccine research and development. *npj Vaccines* **5**, 111 (2020).
10. McMullan, L. K. et al. A new phlebovirus associated with severe febrile illness in Missouri. *N. Engl. J. Med.* **367**, 834–841 (2012).
11. Pastula, D. M. et al. Notes from the field: Heartland virus disease-United States, 2012-2013. *Morb. Mortal. Wkly. Rep.* **63**, 270–271 (2014).
12. Shen, S. et al. A novel tick-borne phlebovirus, closely related to severe fever with thrombocytopenia syndrome virus and Heartland virus, is a potential pathogen. *Emerg. Microbes Infect.* **7**, 1–14 (2018).
13. Fu, Y. et al. Phylogeographic analysis of severe fever with thrombocytopenia syndrome virus from Zhoushan Islands, China: implication for transmission across the ocean. *Sci. Rep.* **6**, 19563 (2016).
14. Yun, S. M. et al. Molecular genomic characterization of tick- and human-derived severe fever with thrombocytopenia syndrome virus isolates from South Korea. *PLoS Negl. Trop. Dis.* **11**, e0005893 (2017).
15. Du, S. et al. Cryo-EM structure of severe fever with thrombocytopenia syndrome virus. *Nat. Commun.* **14**, 6333 (2023).

16. Sun, Z. et al. Architecture of severe fever with thrombocytopenia syndrome virus. *Protein Cell* **14**, 914–918 (2023).
17. Spiegel, M., Plegge, T. & Pöhlmann, S. The role of phlebovirus glycoproteins in viral entry, assembly and release. *Viruses* **8**, 202 (2016).
18. Tani, H. et al. Characterization of glycoprotein-mediated entry of severe fever with thrombocytopenia syndrome virus. *J. Virol.* **90**, 5292–5301 (2016).
19. Zhang, L. et al. CCR2 is a host entry receptor for severe fever with thrombocytopenia syndrome virus. *Sci. Adv.* **9**, eadg6856 (2023).
20. Wu, Y. et al. Structures of phlebovirus glycoprotein Gn and identification of a neutralizing antibody epitope. *Proc. Natl. Acad. Sci. USA.* **114**, E7564–e7573 (2017).
21. Kwak, J. E. et al. Development of a SFTSV DNA vaccine that confers complete protection against lethal infection in ferrets. *Nat. Commun.* **10**, 3836 (2019).
22. Kim, D. et al. Self-assembling Gn head ferritin nanoparticle vaccine provides full protection from lethal challenge of Dabie bandavirus in aged ferrets. *mBio* **14**, e0186823 (2023).
23. Yoshikawa, T. et al. A highly attenuated vaccinia virus strain LC16m8-based vaccine for severe fever with thrombocytopenia syndrome. *PLoS Pathog* **17**, e1008859 (2021).
24. Dong, F. et al. Single dose of a rVSV-based vaccine elicits complete protection against severe fever with thrombocytopenia syndrome virus. *npj Vaccines* **4**, 5 (2019).
25. Kim, J.-Y. et al. mRNA vaccine encoding Gn provides protection against severe fever with thrombocytopenia syndrome virus in mice. *npj Vaccines* **8**, 167 (2023).
26. Kim, K. H. et al. An anti-Gn glycoprotein antibody from a convalescent patient potently inhibits the infection of severe fever with thrombocytopenia syndrome virus. *PLoS Pathog* **15**, e1007375 (2019).
27. Guo, X. et al. Human antibody neutralizes severe Fever with thrombocytopenia syndrome virus, an emerging hemorrhagic Fever virus. *Clin. Vaccine Immunol* **20**, 1426–1432 (2013).
28. Wu, X. et al. A single-domain antibody inhibits SFTSV and mitigates virus-induced pathogenesis in vivo. *JCI Insight* **5**, e136855 (2020).
29. Sankhala, R. S. et al. Zika-specific neutralizing antibodies targeting inter-dimer envelope epitopes. *Cell Rep.* **42**, 112942 (2023).
30. Earnest, J. T. et al. The mechanistic basis of protection by non-neutralizing anti-alphavirus antibodies. *Cell Rep.* **35**, 108962 (2021).
31. Williamson, L. E. et al. Human antibodies protect against aerosolized eastern equine encephalitis virus infection. *Cell* **183**, 1884–1900.e1823 (2020).
32. Engdahl, T. B. et al. Antigenic mapping and functional characterization of human New World hantavirus neutralizing antibodies. *Elife* **12**, e81743 (2023).
33. Wang, Q. et al. Molecular determinants of human neutralizing antibodies isolated from a patient infected with Zika virus. *Sci. Transl. Med.* **8**, 369ra179 (2016).
34. Chi, X. et al. A neutralizing human antibody binds to the N-terminal domain of the Spike protein of SARS-CoV-2. *Science* **369**, 650–655 (2020).
35. Song, P. et al. Deficient humoral responses and disrupted B-cell immunity are associated with fatal SFTSV infection. *Nat. Commun.* **9**, 3328 (2018).
36. Zhao, H. et al. Structural basis of zika virus-specific antibody protection. *Cell* **166**, 1016–1027 (2016).
37. Zhao, H. et al. Mechanism of differential Zika and dengue virus neutralization by a public antibody lineage targeting the DIII lateral ridge. *J. Exp. Med.* **217**, e20191792 (2020).
38. Robbiani, D. F. et al. Recurrent potent human neutralizing antibodies to zika virus in Brazil and Mexico. *Cell* **169**, 597–609.e511 (2017).
39. Yuan, M. et al. Structural basis of a shared antibody response to SARS-CoV-2. *Science* **369**, 1119–1123 (2020).
40. Yuan, M. et al. Molecular analysis of a public cross-neutralizing antibody response to SARS-CoV-2. *Cell Rep.* **41**, 111650 (2022).
41. Stass, R. et al. Mechanistic basis for potent neutralization of Sin Nombre hantavirus by a human monoclonal antibody. *Nat Microbiol.* **8**, 1293–1303 (2023).
42. Chapman, N. S. et al. Potent neutralization of Rift Valley fever virus by human monoclonal antibodies through fusion inhibition. *Proc. Natl. Acad. Sci. USA* **118**, e2025642118 (2021).
43. Wang, L. et al. The tick saliva peptide HIDfsin2 promotes the tick-borne virus SFTSV replication in vitro by enhancing p38 signal pathway. *Arch. Toxicol.* **97**, 1783–1794 (2023).
44. Nie, J. et al. Quantification of SARS-CoV-2 neutralizing antibody by a pseudotyped virus-based assay. *Nat. Protoc.* **15**, 3699–3715 (2020).
45. Xiong, Q. et al. Close relatives of MERS-CoV in bats use ACE2 as their functional receptors. *Nature* **612**, 748–757 (2022).
46. Lefrancios, L. & Lyles, D. S. The interactionof antiody with the major surface glycoprotein of vesicular stomatitis virus. I. Analysis of neutralizing epitopes with monoclonal antibodies. *Virology* **121**, 157–167 (1982).
47. Whelan, S. P., Ball, L. A., Barr, J. N. & Wertz, G. T. Efficient recovery of infectious vesicular stomatitis virus entirely from cDNA clones. *Proc. Natl Acad. Sci. USA* **92**, 8388–8392 (1995).
48. von Boehmer, L. et al. Sequencing and cloning of antigen-specific antibodies from mouse memory B cells. *Nat. Protocols* **11**, 1908–1923 (2016).
49. Tiller, T. et al. Efficient generation of monoclonal antibodies from single human B cells by single cell RT-PCR and expression vector cloning. *J Immunol. Methods* **329**, 112–124 (2008).
50. Matumoto, M. A note on some points of calculation method of LD50 by Reed and Muench. *Jpn. J. Exp. Med.* **20**, 175–179 (1949).
51. Gildea, R. J. et al. xia2.multiplex: a multi-crystal data-analysis pipeline. *Acta Crystallogr. D: Struct. Biol.* **78**, 752–769 (2022).
52. Kabsch, W. XDS. *Acta Crystallogr. D: Biol. Crystallogr.* **66**, 125–132 (2010).
53. Winter, G. et al. DIALS as a toolkit. *Protein Sci.* **31**, 232–250 (2022).
54. Evans, P. R. & Murshudov, G. N. How good are my data and what is the resolution? *Acta Crystallogr. D: Biol. Crystallogr.* **69**, 1204–1214 (2013).
55. Winn, M. D. et al. Overview of the CCP4 suite and current developments. *Acta Crystallogr. D: Biol. Crystallogr.* **67**, 235–242 (2011).
56. McCoy, A. J. et al. Phaser crystallographic software. *J. Appl. Crystallogr.* **40**, 658–674 (2007).
57. Jumper, J. et al. Highly accurate protein structure prediction with AlphaFold. *Nature* **596**, 583–589 (2021).
58. Emsley, P. & Cowtan, K. Coot: model-building tools for molecular graphics. *Acta Crystallogr. D: Biol. Crystallogr.* **60**, 2126–2132 (2004).
59. Adams, P. D. et al. PHENIX: a comprehensive Python-based system for macromolecular structure solution. *Acta Crystallogr. D: Biol. Crystallogr.* **66**, 213–221 (2010).
60. Navaratnarajah, C. K., Rosemarie, Q. & Cattaneo, R. A structurally unresolved head segment of defined length favors proper measles virus hemagglutinin tetramerization and efficient membrane fusion triggering. *J. Virol.* **90**, 68–75 (2016).
61. Sun, Y. et al. Early diagnosis of novel SFTS bunyavirus infection by quantitative real-time RT-PCR assay. *J. Clin. Virol.* **53**, 48–53 (2012).
62. Müller, U. et al. Functional role of type I and type II interferons in antiviral defense. *Science* **264**, 1918–1921 (1994).

Acknowledgements

The authors thank Dr. Huan Yan and Xue-jie Yu for providing the reagents and Dr. Leike Zhang for providing the IFN-α/β receptor knockout mice. We acknowledge the staff of the BL02U1 and BL10U2 beamlines at Shanghai Synchrotron Radiation Facility (Shanghai, People's Republic of China) for assistance during data collection. We are grateful to Dr. Yin Liu

(Medical Research Institute, Wuhan University) for technical support in single-cell sorting and Dr. Fei Deng (National Virus Resource Center, China) for providing the virus strain HBMC5. This work was supported by National Natural Science Foundation of China (82172268 to H.Z. and 32170171 to Y.N.), Hubei Province health and family planning scientific research project (WJ2023Q007 to H.Z.), the CAS Pioneer Hundred Talents Program to Z.D., CAS Youth Interdisciplinary Team to H.Z. and Y.H., and the Youth Innovation Promotion Association of Chinese Academy of Sciences to Y.N.

Author contributions

H.Z., Z.D., and Y.N. supervised the project. X.R. conducted the biochemical preparations and functional assays with the help of F.Y., B.W., and S.Y.; J.S. and W.D. performed authentic virus neutralization assay and animal experiment; Z.X. conducted the IFN-α/β receptor-knockout mouse breeding. W.K., Z.D., and Y.W. determined the crystal structures. X.R., J.S., Y.H., H.W., Z.D., Y.N., and H.Z. analyzed the data. H.Z. and Z.D. wrote the manuscript with input from all authors.

Competing interests

The authors declare no competing interests.

Additional information

Supplementary information The online version contains supplementary material available at https://doi.org/10.1038/s41467-024-51108-z.

Correspondence and requests for materials should be addressed to Zengqin Deng, Yun-Jia Ning or Haiyan Zhao.

Peer review information *Nature Communications* thanks the anonymous, reviewer(s) for their contribution to the peer review of this work. A peer review file is available.

Reprints and permissions information is available at http://www.nature.com/reprints

Publisher's note Springer Nature remains neutral with regard to jurisdictional claims in published maps and institutional affiliations.

Open Access This article is licensed under a Creative Commons Attribution-NonCommercial-NoDerivatives 4.0 International License, which permits any non-commercial use, sharing, distribution and reproduction in any medium or format, as long as you give appropriate credit to the original author(s) and the source, provide a link to the Creative Commons licence, and indicate if you modified the licensed material. You do not have permission under this licence to share adapted material derived from this article or parts of it. The images or other third party material in this article are included in the article's Creative Commons licence, unless indicated otherwise in a credit line to the material. If material is not included in the article's Creative Commons licence and your intended use is not permitted by statutory regulation or exceeds the permitted use, you will need to obtain permission directly from the copyright holder. To view a copy of this licence, visit http://creativecommons.org/licenses/by-nc-nd/4.0/.

© The Author(s) 2024